Molecular Mechanism of Spectral Tuning in Sensory Rhodopsin II[†]

Lei Ren,[‡] Charles H. Martin,[‡] Kevin J. Wise,[‡] Nathan B. Gillespie,[‡] Hartmut Luecke,[§] Janos K. Lanyi,[‖]
John L. Spudich,[⊥] and Robert R. Birge*,[‡]

*Departments of Chemistry and of Molecular and Cell Biology, University of Connecticut, 55 North Eagleville Road,
Storrs, Connecticut 06269, W. M. Keck Center for Molecular Electronics, Syracuse University, 111 College Place,
Syracuse, New York 13244, Department of Molecular Biology and Biochemistry, University of California,
Irvine, California 92697, Department of Physiology and Biophysics, University of California, Irvine, California 92697, and
Department of Microbiology and Molecular Genetics and Structure Biology Center, University of Texas Medical School,
Houston, Texas 77030*

ABSTRACT: Sensory rhodopsin II (SRII) is unique among the archaeal rhodopsins in having an absorption maximum near 500 nm, blue shifted roughly 70 nm from the other pigments. In addition, SRII displays vibronic structure in the λ_{max} absorption band, whereas the other pigments display fully broadened band maxima. The molecular origins responsible for both photophysical properties are examined here with reference to the 2.4 Å crystal structure of sensory rhodopsin II (NpSRII) from *Natronobacterium pharaonis*. We use semiempirical molecular orbital theory (MOZYME) to optimize the chromophore within the chromophore binding site, and MNDO-PSDCI molecular orbital theory to calculate the spectroscopic properties. The entire first shell of the chromophore binding site is included in the MNDO-PSDCI SCF calculation, and full single and double configuration interaction is included for the chromophore π-system. Through a comparison of corresponding calculations on the 1.55 Å crystal structure of bacteriorhodopsin (bR), we identify the principal molecular mechanisms, and residues, responsible for the spectral blue shift in NpSRII. We conclude that the major source of the blue shift is associated with the significantly different positions of Arg-72 (Arg-82 in bR) in the two proteins. In NpSRII, this side chain has moved away from the chromophore Schiff base nitrogen and closer to the β-ionylidene ring. This shift in position transfers this positively charged residue from a region of chromophore destabilization in bR to a region of chromophore stabilization in NpSRII, and is responsible for roughly half of the blue shift. Other important contributors include Asp-201, Thr-204, Tyr-174, Trp-76, and W402, the water molecule hydrogen bonded to the Schiff base proton. The W402 contribution, however, is a secondary effect that can be traced to the transposition of Arg-72. Indeed, secondary interactions among the residues contribute significantly to the properties of the binding site. We attribute the increased vibronic structure in NpSRII to the loss of Arg-72 dynamic inhomogeneity, and an increase in the intensity of the second excited $^1A_g*^-$-like state, which now appears as a separate feature within the λ_{max} band profile. The strongly allowed $^1B_u*^+$-like state and the higher-energy $^1A_g*^-$-like state are highly mixed in NpSRII, and the latter state borrows intensity from the former to achieve an observable oscillator strength.

Membrane-bound light-transducing proteins based on retinal are found in unicellular eukaryotes (*1*), eubacteria (*2*), and archaea (*3–5*). These proteins all share a common motif of seven transmembrane helices enclosing an interior chromophore binding site. The photoactive moiety is retinal attached to the seventh helix via a Schiff base linkage to a conserved lysine. Upon absorption of light, the chromophore isomerizes to store the electrostatic and conformational energy necessary to drive the dark reactions that carry out either light-driven ion transport or photosensory signaling (*1, 4, 6*). Halophilic archaea have both types of light-transducing proteins, including the proton pump bacterio-rhodopsin (BR),[1] the chloride pump halorhodopsin (HR), and the phototaxis pigments sensory rhodopsin I (SRI) and II (SRII or phoborhodopsin).

While BR, HR, and SRI have absorption maxima that fall in a relatively narrow range (560–590 nm), SRII has an absorption maximum at ~500 nm. This wavelength corresponds to the wavelength maxima of the vertebrate and

[1] Abbreviations: BR, bacteriorhodopsin from *Halobacterium salinarum*; bR or bR(LA), light-adapted bacteriorhodopsin; MNDO-PSDCI, modified neglect of differential overlap with partial single and double configuration interaction; MOZYME, semiempirical molecular orbital procedure that is designed to carry out self-consistent field calculations on proteins; n_D, refractive index at the sodium D line; NpSRII, sensory rhodopsin II from *Natronobacterium pharaonis*; PM3, parameterization of MOPAC.

invertebrate visual pigments responsible for scotopic (low-light) vision (*7*). Not only does SRII exhibit a large blue shift relative to BR, HR, and SRI, but it also displays an unusual vibronic structure in the λ_{max} absorption band (*8–12*). The other pigments display virtually no vibronic development in the λ_{max} band, even when the temperature is reduced to <77 K (*13–15*). The unusual spectroscopic properties of SRII are all the more intriguing because BR, HR, SRI, and SRII are significantly homologous. Shimino et al. examined 23 archaeal rhodopsins, and noted that there are three residues within the binding site region which are rigorously conserved in all the sensory rhodopsin II sequences but which differ in the BR, HR, and SRI proteins (*16*). These are Val-108, Gly-130, and Thr-204 (position numbers refer to the NpSRII sequence). These authors replaced all three residues with their sequential counterparts in bacteriorhodopsin (V108M, G130S, and T204A), but observed an only 15 nm red shift (*16*). These investigators concluded that the major source of the blue shift was yet to be determined, and likely involved a change in the protein geometry (*16*).

The unusual spectroscopic properties of SRII have been addressed from a variety of perspectives in previous studies (*8, 9, 12, 16–35*). The most recent studies are based on the two high-resolution crystal structures that have recently been published (*17, 18*). The study of Luecke et al. (*17*) is based on the 2.4 Å structure discussed in the same paper and deposited in the Protein Data Bank as entry 1JGJ. The study by Hayashi et al. (*18*) is based on a separate set of coordinates from the crystal structure studies of Royant et al. (*36*). The study presented here and the Hayashi study (*18*) come to different conclusions about the principal mechanism of spectral tuning, as we discuss below.

METHODS

The methods and procedures for generating the 2.4 Å structure of NpSRII have been described separately (*17*). We added hydrogens to this structure by using the HBuild command in CHARMM (*37*), assuming that the Schiff base is protonated, Asp-75, Asp-193, and Asp-201 are negatively charged, and Arg-72 is positively charged. These assignments are all evident from the analogy to the bR assignment, with the exception of Asp-193. A ground-state MOZYME calculation indicated that Asp-193 forms a strong electrostatic interaction with Arg-72 (see the discussion below). All other ionic residues were made neutral, an approach that is recommended in studies of this kind when a full pK_a analysis is not available. This approach serves to simulate neutralization of charges at the surface due to counterions, and avoids generating an artificial electric field through the binding site that is associated with incorrect surface charge assumptions. We tested the sensitivity of our calculations to this assumption and noted that charge assignments for Glu-122 and Arg-123, which are within 10.8 and 7.8 Å of ring C3 of the chromophore, respectively, do have a small impact on the calculated absorption maximum of the chromophore. But the effect is small, and the impact is negligible with respect to the principal conclusions of this study. The hydrogen atoms were minimized by using the PM3 Hamiltonian within MOZYME, a version of MOPAC that can handle entire proteins (*38–40*). All non-hydrogen atoms were held fixed

during this minimization. Following hydrogen minimization, the chromophore (but not the lysine residue to which it is linked) and all the hydrogen atoms were minimized using the PM3 Hamiltonian. We favor the PM3 parametrization over AM1, because the PM3 Hamiltonian provides a better description of water (*41*) and of retinal chromophores (*42, 43*). A second minimization of the hydrogen atoms was carried out to permit additional relaxation of these atoms in response to chromophore movement. Note that although we minimized the chromophore, we held the terminal nitrogen atom (NZ of Lys-205) fixed at the crystal geometry. It is necessary to optimize the chromophore because the MNDO-PSDCI calculations are extremely sensitive to small variations in bond lengths and bond angles within the delocalized π-system. By minimizing the chromophore and hydrogen atoms alone, we guarantee that the results we obtain are fully consistent with the crystal structure. Minimization of the chromophore removes the minor imperfections in the chromophore geometry that are insignificant with respect to overall structure, but are highly significant to the calculated photophysical properties.

A structure of bacteriorhodopsin including hydrogen was prepared using the 1.55 Å crystal structure (*44*) and the same procedures as described above for NpSRII. We assumed that Arg-82(+), Asp-85(−), Glu-204(−), Asp-212(−), and the chromophore Schiff base were charged. We selected Glu-204 rather than Glu-194 to carry the negative charge, because the E204(−)–E194 pairing was calculated to be lower in energy. Our results and conclusions are insensitive to the choice, provided only one of these residues (E204 or E194) is charged.

The photophysical properties of the bound chromophore were calculated using MNDO-PSDCI molecular orbital theory (*42, 43, 45–48*). Although we have developed parametrizations for MNDO, AM1, and PM3 Hamiltonians, we selected the PM3 parametrization to be consistent with the ground state minimization methods. We also have confidence in this parametrization because it does a reasonably good job of reproducing the spectroscopic properties of rhodopsin. For example, the MNDO-PSDCI (PM3) absorption maximum of rhodopsin is predicted at 488 nm (*43*) on the basis of the crystal structure (*49*), in good agreement with that found in the experiment (498 nm). To reduce the calculation to a tractable size, we selected only the first shell of the binding site for inclusion in the self-consistent field (SCF) treatment. The first shell was defined to include all residues or water molecules located within 5.6 Å of any of the chromophore atoms, in addition to any charged residue within 12 Å. The key binding site residues for the NpSRII calculation are shown in, or defined in the caption of, Figure 1. The binding site for bacteriorhodopsin was selected in an analogous fashion and explicitly defined in the footnotes of Table 1. All of our calculations used full single and double CI within the π-manifold of the protonated Schiff base chromophore. When we included dispersion in the calculation, we included full single and double CI on the aromatic residues as well, which simulates the dispersive interaction between the residue and the chromophore via the double excitations that occur simultaneously across the two chromophoric moieties. Such calculations rapidly expand the basis set, and we were forced to use extrapolation methods to do the full dispersion calculation which included

FIGURE 1: Key binding site residues in sensory rhodopsin II (NpSRII) from *Natronobacterium pharaonis*. Residues behind the plane of the chromophore are shown in gray. A number of small, aliphatic residues (Ala-47, Val-108, Ala-111, Gly-112, Leu-126, Gly-130, Ala-131, and Ala-172) are not shown to permit viewing of other residues more relevant to wavelength regulation. Only selected hydrogen atoms are shown.

Table 1: Spectroscopic and Dipolar Properties of the Protein-Bound Chromophores in NpSRII and bR as a Function of Binding Site Environment

property	NpSRII		bR(LA)	
	residues and method[a]	value	residues and method[b]	value
$\Delta E(S_1)$	just chromophore	1.650 eV (751 nm, $f = 0.69$)	just chromophore	1.641 eV (756 nm, $f = 0.66$)
$\Delta E(S_1)$	D75, D201, H_2O	2.696 eV (459 nm, $f = 0.56$)	D85, D212, H_2O	2.616 eV (473 nm, $f = 0.63$)
$\Delta E(S_1)$	R72, D75, D201, H_2O	2.740 eV (452 nm, $f = 0.69$)	R82, D85, D212, H_2O	2.436 eV (509 nm, $f = 0.48$)
$\Delta E(S_1)$	full BS (ES)	2.768 eV (447 nm, $f = 0.80$)	full BS (ES)	2.490 eV (498 nm, $f = 0.70$)
$\Delta E(S_2)$	full BS (ES)	3.188 eV (388 nm, $f = 0.65$)	full BS (ES)	3.113 eV (398 nm, $f = 0.44$)
$\Delta E(S_1)$	full BS (ES and disp)	2.648 eV (468 nm, $f = 0.80$)	full BS (ES and disp)	2.338 eV (530 nm, $f = 0.70$)
$\Delta E(S_2)$	full BS (ES and disp)	3.091 eV (401 nm, $f = 0.65$)	full BS (ES and disp)	3.019 eV (410 nm, $f = 0.44$)
$\Delta E(S_2) - \Delta E(S_1)$	full BS (ES and disp)	0.443 eV	full BS (ES and disp)	0.681 eV
$\Delta\mu[\mu(S_1) - \mu(S_0)]$	neutral BS (ES)	12.349 D	neutral BS (ES)	8.359 D
$\Delta\mu[\mu(S_2) - \mu(S_0)]$	neutral BS (ES)	3.455 D	neutral BS (ES)	2.127 D

[a] The same chromophore geometry, as generated through optimization (MOZYME/PM3) within the full binding site, was used for all calculations. The MNDO-PSDCI calculations included full single and double configuration interaction (CI) from the chromophore π-system, and the dispersive calculations added single and double CI on Trp-76, Trp-171, and Tyr-174. When H_2O is listed, all three water molecules near the Schiff base were included (Figure 1). When the full binding site (full BS) was included, all the residues shown in Figure 1 were included in the SCF calculation. To calculate the dipole moment changes, a neutral site was generated by excluding Asp-193. Abbreviations: ES, electrostatics only, as represented within the SCF calculations; disp, dispersion as reflected in double CI across chromophore and aromatic residues. [b] Global assumptions and abbreviations as in footnote a. The MNDO-PSDCI calculations included full single and double CI from the chromophore π-system, and the dispersive calculations added single and double CI on Trp-86, Trp-182, and Tyr-185. When the full binding site was included, the following residues were included: M20, V49, A53, Y57, R82(+), Y83, D85(−), W86, T89, T90, L93, M118, I119, G122, L123, W137, W138, S141, T142, M145, W182, S183, Y185, P186, W189, E194, E204(−), F208, D212(−), A215, and LYR216(+), in addition to all water molecules within 6 Å of the chromophore. To calculate the dipole moment changes, a neutral site was generated by excluding Glu-204.

CISD involving the π-systems of Trp-76, Trp-171, and Tyr-174. Such extrapolations are reliable for transition energies, but not for oscillator strengths, and so we report all oscillator strengths with reference to the "nondispersive" basis set.

RESULTS AND DISCUSSION

We used two approaches to examine the mechanism of spectral tuning in NpSRII and bR. [We will use the abbreviation bR, or bR(LA), to indicate light-adapted (*all-trans*) BR. NpSRII does not undergo light−dark adaptation

(*28*).] In the first approach, we built up the structure from the chromophore in sections to observe the impact of individual residues, or groups of residues, on the photo-physical properties of the chromophore. These results are presented in Table 1. In the second approach, we started from the full binding site (constructed as described above), replaced selected residues with glycine, and recalculated the transition energies. If the residue being replaced was charged, the hydrogen atoms were reminimized to more accurately reflect the influence of dipole−dipole and hydrogen-bonding interactions on the energetics. These results are presented in Table 2.

Table 2: Spectral Tuning of the Absorption Maximum in NpSRII and bR as a Function of Residue

	NpSRII		bR(LA)		NpSRII−bR
origin of shift[a]	residue	$\Delta E(S_1)$ (eV)	residue	$\Delta E(HCS_1)$ (eV)	$\Delta\Delta E(S_1)$ (eV)
ES	Asp-75	0.548	Asp-85	0.550	−0.002
ES	Asp-201	0.375	Asp-212	0.328	0.047
ES	Arg-72	0.044	Arg-82	−0.180	0.224
ES	Thr-204	0.046	Ala-215	0.003	0.043
ES	W402	0.274	W402	0.258	0.016
disp	Trp-76	−0.070	Trp-86	−0.086	0.016
disp	Trp-171	−0.020	Trp-182	−0.017	−0.003
disp	Tyr-174	−0.031	Tyr-185	−0.049	0.018
net shift[b]		1.167		0.808	0.359
observed[c]					0.314

[a] The origin of the spectral shift is either electrostatic (ES) or dispersive (disp). All data are given for the lowest-lying, strongly allowed ^1B_u-like excited singlet state, which is responsible for the λ_{max} absorption band. [b] The net shift is given in electron volts, and is relevant only to those residues listed. The shifts, when added, are expected to overestimate the net shift because these values include only first-order effects and ignore second-order effects and mediation by other residues in the binding site. [c] The observed energy shift of NpSRII relative to light-adapted bacteriorhodopsin is calculated as follows: ΔE(NpSRII, λ_{max}=498 nm) = 2.490 eV, ΔE(bR, λ_{max}=570 nm) = 2.175 eV, and $\Delta\Delta E$ = 0.314 eV.

Role of Chromophore Geometry in Spectral Tuning. A logical place to start our investigation is to look at the potential role of chromophore geometry in blue-shifting SRII. The crystal structure reveals significant differences in the tilt and slant of the polyene chain in SRII relative to that in bacteriorhodopsin (*17*). As shown in Table 1, however, there is no significant difference between the transition energies of the two chromophores. One might suggest that our use of optimized chromophores will mask any effect that chromophore geometry might have on the transition energy. We reject that suggestion for three reasons. First, the optimization took place within the protein binding site. Second, our optimized structures overlap nicely with the crystal structures and are "visually identical". Third, our calculations based on the optimized chromophore structures reproduce ~90% of the observed blue shift. We conclude that changes in chromophore structure are of minor consequence in defining the spectral tuning differences between NpSRII and bR. This observation is in good agreement with the conclusions of Hayashi et al. (*18*).

Role of the Counterions in Spectral Tuning. The counterion structure of bacteriorhodopsin is quite unusual, and involves a quadrapole system that consists of the protonated chromophore, Asp-85, Asp-212, and Arg-82 (*44*). The importance of Arg-82 in defining the electrostatic environment of the chromophore has been emphasized before (*42*), and previous MNDO-PSDCI calculations indicate that it is responsible for a red shift in the λ_{max} band of 0.3−0.5 eV (see Table 2 of ref *42*). An alternative method of blue shifting the λ_{max} band, however, is to move Asp-85 or Asp-212 closer to the Schiff base nitrogen, which would preferentially stabilize the ground state (*18*). An evaluation of these possibilities as they apply to NpSRII versus bR is presented in Figure 2. Here we show the observed distances of the carboxylate oxygens of Asp-75 and Asp-201 (and their homologues in bR) from the Schiff base nitrogen. We also show the distance of the principal water molecule (W402) from the Schiff base nitrogen, a value which will turn out to be more important than one might
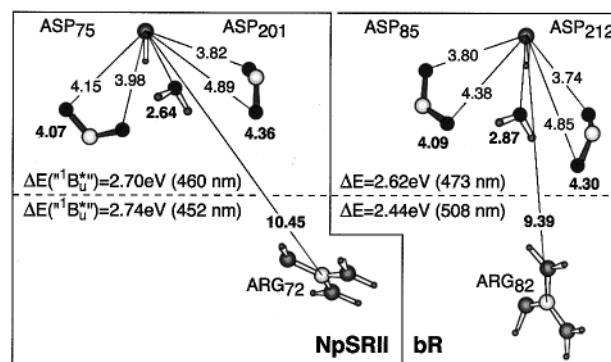

FIGURE 2: Comparison of the key distances (angstroms) that define the electrostatic interactions among the conserved aspartic acid residues and the arginine residue near the Schiff base nitrogen in NpSRII (left) and light-adapted bacteriorhodopsin (right). All distances are from the Schiff base nitrogen, and in the case of the Asp residues, the individual distances to the carboxylate oxygens are averaged and shown in boldface underneath the residue. The transition energy data above the dotted line is for a calculation including the chromophore, the two Asp residues, and all three waters in the region. The corresponding data below the dashed line include, in addition to the molecules listed above, the Arg residue. The atomic positions for bR were taken from the 1.55 Å crystal structure (see the text).

anticipate. Finally, we show the distance of the central carbon atom of the side chain of Arg-72 (Arg-82 in bR) from the Schiff base nitrogen. If calculations are performed on these residues alone, the results provide a perspective on the principal mechanism of spectral tuning. When only the two Asp residues and water are included, NpSRII is blue shifted relative to bR, but by only 0.08 eV (13 nm). (Note that we included all three water molecules in the Schiff base region in this calculation.) If, however, we add Arg-72 (or Arg-82 in bR) to the calculation, we generate a blue shift of NpSRII but a red shift of bR. Now, the calculated absorption maximum of NpSRII is blue shifted relative to bR by 0.30 eV, very close to the observed value of 0.31 eV. Clearly, Arg-72 is the key to understanding the differential spectral shift. But how is it possible that the relatively distant Arg-72 residue can be responsible for a blue shift in NpSRII? To understand this phenomenon, we need to examine the electrostatics of the excitation process.

The ground state of the protonated Schiff base chromophore concentrates the net positive charge near the two Asp counterions, as is evident from an evaluation of the electrostatic contours shown in Figure 3. Arg-82 destabilizes the chromophore in bacteriorhodopsin indirectly by stabilizing Asp-85 and Asp-212, which forces these two residues to distribute their negative charge further away from the Schiff base nitrogen. The situation is very different in NpSRII. Arg-72 is pointed away from the binding site to form an electrostatic bridge to Asp-193 (Figure 3A). This interaction indirectly stabilizes the chromophore by allowing Asp-75 and Asp-201 to distribute a majority of their negative charge toward the chromophore. Thus, even though Asp-201 is farther from the Schiff base nitrogen in NpSRII than is Asp-212 from the Schiff base nitrogen in bR (Figure 2), Asp-201 provides 0.047 eV of enhanced stabilization relative to its counterpart in bR (Table 2). This second-order effect is due to electron redistribution rather than molecular reorganization, and can only be described properly when the
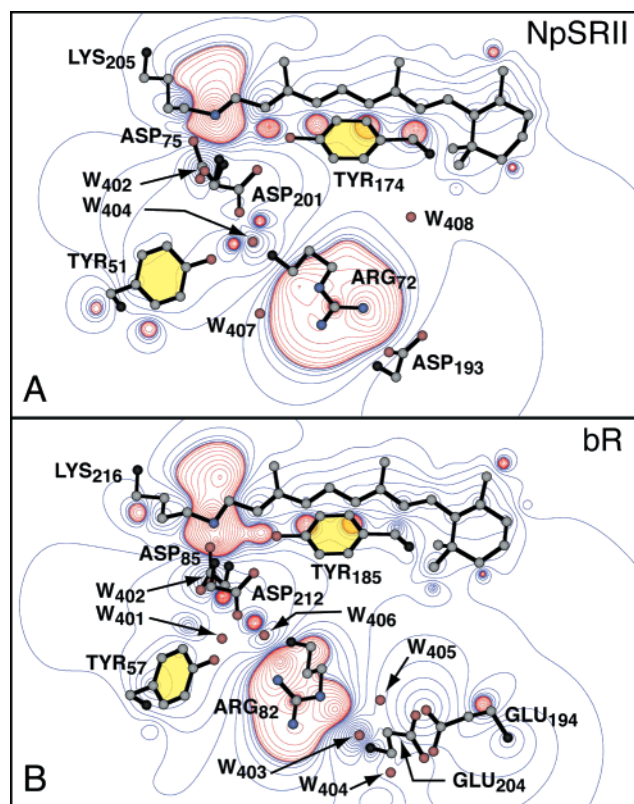
FIGURE 3: Ground-state electrostatic fields in the plane of the chromophores in NpSRII (A) and bR (B). The red contours indicate a field associated with excess positive charge, and the blue contours indicate a field associated with excess negative charge.
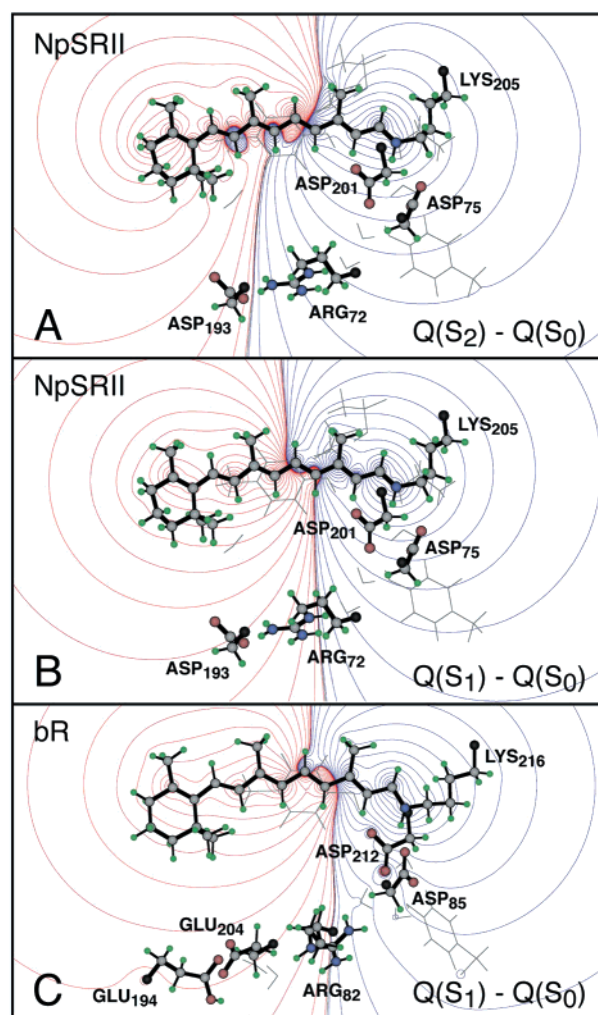

FIGURE 4: Change in the electrostatic fields in the plane of the chromophore upon excitation into the second excited $^1A_g*^-$-like state (A) and the lowest-lying $^1B_u*^+$-like state (B) in NpSRII, with the latter field change compared to that generated via the comparable transition in bR (C). The red contours indicate an increase in positive charge, and the blue contours indicate an increase in negative charge. Note that the side chains of Arg-72 in NpSRII (B) and Arg-82 in bR (C) are on opposite sides of the null-field contour, which explains why Arg-82 red shifts bR but Arg-72 blue shifts NpSRII.

entire binding site is included in the self-consistent field molecular orbital treatment.

Excitation into the lowest-lying strongly allowed $^1B_u*^+$-like excited singlet state transfers negative charge from the ring portion into the Schiff base linkage region of the chromophore. Differential field contours accompanying excitation are shown in Figure 4. The electrostatic field contours shown in Figure 4 are generated by assigning to each atom the change in charge upon excitation into either S_1 (B or C) or S_2 (A), and then drawing the electrostatic field contours in the normal fashion. Thus, these contours show the change in the electrostatic field that accompanies excitation. As can be seen by comparing panels B and C, the S_1 charge shift is very similar in both bR and NpSRII. What is significantly different, however, is the interaction of the respective arginine residues with the differential field. In bacteriorhodopsin, the centroid of the positive charge of Arg-82 is located within the negative region. Thus, Arg-82, because it is positively charged, "stabilizes" the S_0–S_1 transition in bR, which lowers the transition energy. In contrast, the centroid of the positive charge of Arg-72 is located on the positive side of the differential field in NpSRII. Thus, Arg-72 "destabilizes" the S_0–S_1 transition in NpSRII, which increases the transition energy. We note that the charge centroid is defined largely by the location of the terminal NH_2 groups, where ~74% of the positive charge is localized (for the two arginine residues examined here). We conclude that the change in the position of Arg-72 is the primary source of the blue shift in NpSRII relative to bR. As shown in Table 2, this residue alone is responsible for a blue shift of 0.224 eV, which is >70% of the observed total shift of

0.307 eV. Asp-201 is the next most important residue, contributing a blue shift of 0.047 eV. The third most important residue is Thr-204, which is the subject of the next section.

Role of Residue Replacements in Spectral Tuning. A comparison of the primary sequences of NpSRII and bR indicates that after sequence alignment, there are 15 residues that differ in the binding site region. The following list shows the relevant NpSRII residues directly followed by the bR replacement in parentheses: Ile-43 (Val-49), Ile-83 (Leu-93), Val-108 (Met-118), Met-109 (Ile-119), Ala-111 (Gly-122), Gly-112 (Leu-123), Phe-113 (Val-124), Leu-126 (Trp-137), Phe-127 (Trp-138), Met-129 (Ile-140), Gly-130 (Ser-141), Ala-131 (Thr-142), Phe-134 (Met-145), Ala-172 (Ser-183), and Thr-204 (Ala-215). After removing from this group replacements that are highly similar, we tested each to determine which replacement, if any, was significant to spectral tuning. We found only one that was significant (Thr-204 → Ala-215).

The Thr-204 residue is located ∼3.5 Å from the C13 methyl group (C20) (see Figure 1). The conformationally flexible OH group aligns with the strong dipolar field in this region, and preferentially stabilizes the ground state. We calculate that Thr-204 produces a blue shift of 0.043 eV in NpSRII relative to bR (Table 2). This corresponds to a spectral blue shift of 9 nm, in good agreement with the site-directed mutagenesis studies of Shimino et al. (*16*). The potential role of hydroxyl-containing side chains in blue shifting the absorption spectra of cone pigments has been discussed previously (*50*). However, recent studies have indicated that the position of the hydroxyl residue is an important variable in determining the blue shift (*43*). In the study presented here, we found that the Gly-130 → Ser-141 replacement, which involves residues near the β-ionylidene ring, did not have any significant impact on the absorption maximum, in general agreement with the spectroscopic studies of Shimino et al. (*16*). We were surprised to find no significant impact for the two Leu-126 → Trp-137 or Phe-127 → Trp-138 replacements, because tryptophan has the potential to provide a large dispersive red shift. Our calculations indicate, however, that both of these Trp residues are too far from the π-system of the chromophore to provide an observable dispersive shift (see the discussion below).

In summary then, only one replacement (Thr-204 → Ala-215) is of any significant consequence in blue shifting NpSRII relative to bacteriorhodopsin. The other replacements may well combine to form a large secondary effect, but in terms of single replacements, none has an impact. We do note that, in general, these replacements tend to increase the refractive index of the bacteriorhodopsin binding site, a subject discussed in the next section.

Role of Dispersion in Spectral Tuning. Ground-state dispersive forces arise due to the motion of electrons and the fact that, at any given instant, the electron distribution is not uniform. This creates an instantaneous dipole moment, and this dipole moment can induce a dipole moment in another molecule to create a dipole−dipole interaction. Because the instantaneous dipole moment and the induced dipole moment are in an energetically favorable alignment, this interaction always lowers the energy of the system. The energy of stabilization due to dispersion is given by

$$\Delta E_{AB}(\text{disp}) \approx -\frac{3\alpha_A\alpha_B}{2R_{AB}{}^6}\frac{\Delta E_{ave}^A \Delta E_{ave}^B}{\Delta E_{ave}^A + \Delta E_{ave}^B} \quad (1)$$

where α_A and α_B are the polarizabilities of molecules A and B, respectively, ΔE_{ave}^A and ΔE_{ave}^B are the average transition energies of molecules A and B, respectively, and R_{AB} is the separation between the centroids of the electron densities on molecules A and B (*51*). The average transition energy is usually very close to the first ionization energy (*51*), and that value is often used in the calculation because it can be measured experimentally (*52*). Dispersive forces are of significant importance in describing the effect of environment on electronic transitions, and it is known that these interactions are important in red shifting the absorption spectra of the chromophores in rhodopsin and bacteriorhodopsin (*53, 54*). If we define the chromophore as molecule A, the leading term in the dispersive red shift of the $i \leftarrow 0$ transition due to a single nearby residue, B, is

$$\Delta\Delta E_{i0}^A(\text{disp}) \approx$$

$$-\frac{3\hbar^2 e^2}{48\epsilon_0 m_e}\frac{f_{i0}^A\alpha_B}{R_{AB}{}^6}\frac{(2\Delta E_{ave}^A - \Delta E_{i0}^A)}{\Delta E_{ave}^A(\Delta E_{ave}^A - \Delta E_{i0}^A)} + \ldots \quad (2)$$

where f_{i0}^A is the oscillator strength and ΔE_{i0}^A is the transition energy of the $i \leftarrow 0$ transition. As an example, consider Trp-76, which has the centroid of its extended π-system located only 4.4 Å from the centroid of the chromophore π-system (see Figure 1). Assuming $\Delta E_{i0}^A = 2.48$ eV, $\Delta E_{ave}^A = 10$ eV, $\alpha_B = 21$ Å³, and $f_{i0}^A = 0.8$, we calculate a $\Delta\Delta E_{i0}^A(\text{disp})$ of −0.046 eV. This is equivalent to a shift of ∼10 nm. While this is not a large shift, it is significant that a single residue in the binding site can produce such a large dispersive shift. Indeed, as shown in Table 2, our double CI calculations predict that Trp-76 is individually responsible for a dispersive shift of −0.070 eV (14 nm) in NpSRII.

Noting that eq 2 is an approximation to the full dispersive expansion, we are not surprised that it underestimates the dispersive shift calculated via the CISD treatment. There is another mechanism through which a residue such as Trp-76 can red shift the absorption maximum of a nearby chromophore. Equation 2 describes that portion of the dispersive effect associated with the interaction of a transition dipole with an induced dipole of a nearby polarizable group. There is also a transition dipole−transition dipole term that is missing from eq 2. This term, which is usually called an excitonic interaction, is given by

$$\Delta\Delta E_{i0}^A(\text{exciton}) \approx$$

$$\frac{1}{2}[\Delta E_{j0}^B - \Delta E_{i0}^A - \sqrt{(\Delta E_{j0}^B - \Delta E_{i0}^A)^2 + 4V_{AB}{}^2}] + \ldots \quad (3)$$

where

$$V_{AB}{}^2 \approx \frac{9\hbar^4 e^4}{64\pi^2\epsilon_0{}^2 m_e{}^2}\frac{f_{i0}^A f_{j0}^B}{\Delta E_{i0}^A \Delta E_{j0}^B}\frac{\cos^2(\theta_{AB}^{ij})}{R_{AB}{}^6} \quad (4)$$

and ΔE_{j0}^B is the transition energy of a low-lying strongly allowed transition in the nearby residue, f_{j0}^B is the oscillator strength of this transition, and θ_{AB}^{ij} is the angle between the transition dipole moments of the $i \leftarrow 0$ transition on the chromophore (A) and the $j \leftarrow 0$ transition on the residue (B). Equation 3 will always produce a negative exciton shift for $\Delta\Delta E_{i0}^A$ provided ΔE_{j0}^B is higher in energy than ΔE_{i0}^A and the coupling energy, V_{AB}, is non-zero. If we evaluate the exciton splitting of the chromophore transition due to the L_a transition in Trp-76 ($f_{j0}^B = 0.12$, $\Delta E_{j0}^B = 4.43$ eV, and $\theta_{AB}^{ij} = 21°$), we obtain a $\Delta\Delta E_{i0}^A(\text{exciton})$ of −0.014 eV. The sum of eqs 2 and 3 gives a net red shift of −0.06 eV, in good agreement with the value of −0.07 eV predicted by the double CI calculation.

We have presented the above equations primarily to provide a perspective on the variables that are important in red shifting the chromophore absorption band due to non-electrostatic mechanisms. It has long been known that the formal treatment of dispersive effects is achieved by including double configuration interaction (*55*). That is the approach we used in this study (see Methods). A key advantage

of using CISD to calculate the dispersive shifts is avoidance of the assignment of the many variables that are given in eqs 2 and 3, many of which are subject to uncertainty.

We find that there are three residues which make a significant contribution to the dispersive and excitonic red shifts of the chromophores in NpSRII and bR. These are Trp-76, Trp-171, and Tyr-174 in NpSRII and their homological counterparts Trp-86, Trp-182, and Tyr-185 in BR. No other residue was found to induce a dispersive shift of >0.003 eV in either protein. Although the net dispersive shift is slightly larger in bR than in NpSRII, the difference is small (0.031 eV) and provides only 10% of the differential blue shift in NpSRII. Although these three residues also contribute to the net electrostatic shift (*56*), our calculations indicate that they introduce no significant differential electrostatic shift in NpSRII relative to bR.

Our MNDO-PSDCI calculations predict transition energies for both NpSRII and bR that are too high by ~0.17 eV, even when we include CISD over the chromophore and the three dispersive residues. Our calculations on rhodopsin were more successful, predicting an absorption maximum of 488 nm, representing an error of 0.06 eV. We close this section by suggesting that we are still underestimating the dispersive shift. An alternative approach to calculating the dispersive red shift is to use a continuum model, and treat the binding site as a polarizable medium defined by a reaction field. We will use the equation derived by Liptay (*52*):

$$\Delta\Delta E_{i0}^{A}(\text{disp}) \approx$$

$$-\frac{3\hbar^2 e^2}{4\pi\epsilon_0 m_e} \frac{f_{i0}^{A}}{R_A^{3}} \frac{(2\Delta E_{ave}^{A} - \Delta E_{i0}^{A})}{\Delta E_{ave}^{A}(\Delta E_{ave}^{A} - \Delta E_{i0}^{A})} \frac{n^2 - 1}{2n^2 + 1} + \quad (5a)$$

$$\frac{-3\hbar^2 e^2}{16\pi\epsilon_0 m_e} \frac{1}{R_A^{3}} \frac{\Delta E_{i0}^{A}}{\Delta E_{ave}^{A}(\Delta E_{ave}^{A} - \Delta E_{i0}^{A})} \frac{n^2 - 1}{2n^2 + 1} \quad (5b)$$

where R_A is the cavity radius and n is the refractive index of the binding site. We have calculated the refractive index of the binding site by using the methods and procedures of McMeekin et al. (*57*). The refractive index data from ref *57* were updated using the molar refraction data of Jones (*58*) and the molar volume data of Chothia (*59*). The results are shown in Figure 5, and the revised refractive indices are listed in the caption. We assign the refractive index of the binding site as that value observed for the first shell, which is 5.6 Å (heavy atom distance) out from the edge of the chromophore. Although BR has a refractive index (1.5128) slightly higher than that calculated for NpSRII (1.5037, Figure 5), the difference is small and borders on the anticipated margin of error. The refractive index of bacteriorhodopsin at 600 nm is 1.534 (*60*). Our calculations will underestimate the total refractive index of the protein because we have excluded contributions from the chromophore, which is an important contributor to the net refractive index. If we subtract the average carbon–hydrogen bond length of 1 Å from the 5.6 Å value, we obtain a cavity radius of 4.6 Å. This radial value is identical to the value measured for *all-trans*-retinal in solution (based on a measured cavity volume of 402.4 Å³) (*61*). In the case of NpSRII, eq 5 predicts a dispersive red shift of −0.155 eV ($f_{i0}^{A} = 0.8$, $\Delta E_{i0}^{A} = 2.77$ eV) versus a value of −0.134 eV ($f_{i0}^{A} = 0.7$, $\Delta E_{i0}^{A} = 2.49$ eV) in bR. The
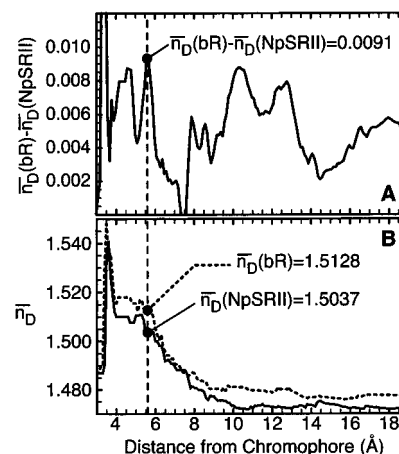

FIGURE 5: Average refractive index (sodium D line) of NpSRII and bR as a function of the distance from the chromophore, with values beyond the edge of the protein held at the surface values so that edge effects are not included. The bottom graph (B) shows the absolute values, while the top graph (A) shows the difference between bR and NpSRII. The values assigned at 5.6 Å represent the average refractive indices (B) or difference (A) for the first shell of the binding site, and indicate that bR has a slightly larger refractive index than NpSRII. The calculations were carried out assuming the following refractive indices for the amino acids (see the text): Ala (1.44080), Arg (1.4904), Asn (1.5008), Asp (1.4948), Cys (1.4909), Gln (1.4836), Glu (1.4842), Gly (1.4675), His (1.5259), Ile (1.4333), Leu (1.4308), Lys (1.4716), Met (1.4909), Phe (1.51548), Pro (1.4365), Ser (1.4943), Thr (1.4684), Trp (1.5826), Tyr (1.5483), and Val (1.4336).

key difference is that NpSRII has a larger oscillator strength than bR. It is interesting to note that the continuum approach predicts a dispersive shift for the entire NpSRII binding site (−0.155 eV) very similar to the net shift calculated via CISD methods for the three major dispersive residues (−0.121 eV, Table 2). Naturally, we would be double counting if we were to add both of these values together, but we note that much of our net error of 0.17 eV may be associated with a neglect of continuum dispersion. We conclude that the ultimate approach to this problem will be found in a combination of CISD and adjusted continuum models. One possibility would be to combine the hybrid methods proposed by Houjou et al. with a discrete calculation of the exciton contributions. Further work in this area is needed, as the above calculations illustrate the difficulty and inadequacy of the current dispersion methods. Our calculations provide ample evidence that any differences in the dispersive shifts in NpSRII versus bR are small.

Origin of the Vibronic Structure in NpSRII. As noted above, sensory rhodopsin II is unique in displaying vibronic structure, or what appears to be vibronic structure, in the λ_{max} absorption band (*8–12*) (see Figure 6A). When the separation in the vibronic bands is assigned by using a least-squares fit to log-normal bands, we find that the maxima do not follow any clear vibronic trend. Although our vibronic separations differ somewhat from the comparable assignment of Chizhov et al. (*12*), both of our studies agree that the A–B separation is ~200 cm⁻¹ smaller than the B–C separation. This observation suggests that band C is not associated with the same progression as bands A and B, and may be associated with a different electronic state. Hayashi et al. have made the interesting suggestion that band C or D might be associated with the low-lying $^1A_g^{*-}$ -like state (*18*).
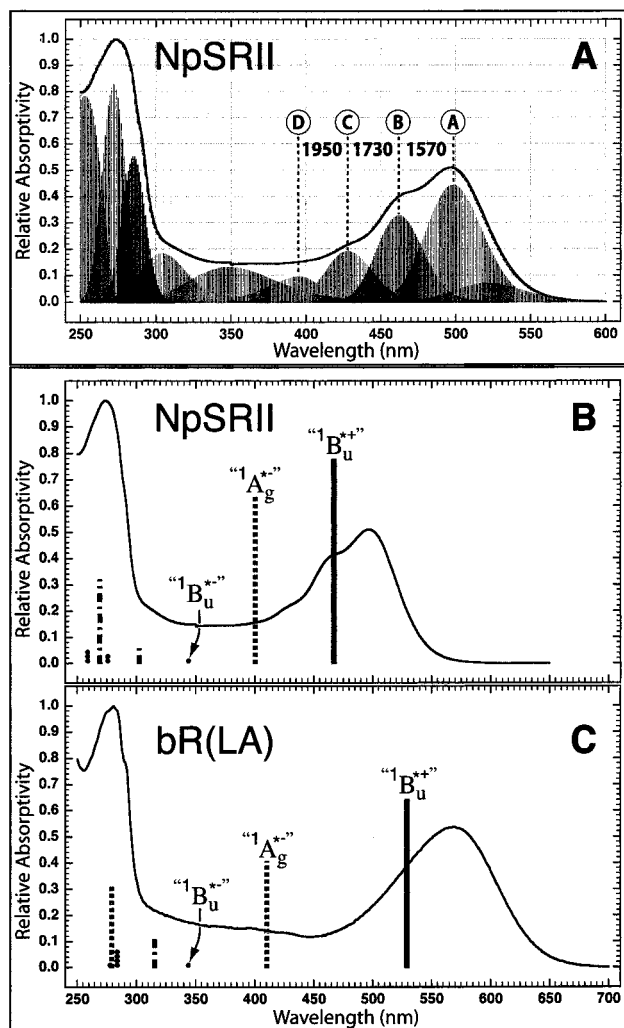
FIGURE 6: Analysis of the spectral features of NpSRII (A and B) and bR (C) with respect to vibronic structure (A) and of the MNDO-PSDCI predictions of the location and intensities of the electronic transitions (B and C). Separations of the vibronic bands in NpSRII (A) are given in wavenumbers based on a least-squares fit of the spectrum to log-normal bands. Only transitions involving the chromophore are shown in panels B and C, and the symmetry assignments are very approximate.

We agree and provide additional evidence for this assignment. The MNDO-PSDCI energies and intensities of the low-lying $\pi\pi^*$ states of the chromophores in NpSRII and bR are superimposed on the absorption spectra in Figure 6. This figure shows clearly that our calculations predict that the $^1A_g^{*-}$-like state is closer to the lowest-lying $^1B_u^{*+}$-like state in NpSRII, and further that it has a much higher intensity (also see Table 1). The location and properties of the $^1A_g^{*-}$-like state in bacteriorhodopsin have been assigned by using two-photon spectroscopy (*62*). The two-photon maximum of the $^1A_g^{*-}$-like ($f_{obs} \approx 0.3$) is at 474 nm, 0.44 eV above that of the $^1B_u^{*+}$-like ($f_{obs} \approx 0.8$) state. Our calculations predict the $^1A_g^{*-}$-like ($f_{calcd} = 0.44$) state is at 420 nm, 0.68 eV above the $^1B_u^{*+}$-like ($f_{calcd} = 0.7$) state (Table 1). Thus, our calculations tend to overestimate both the oscillator strength of the $^1A_g^{*-}$-like state and the energy of this state above the $^1B_u^{*+}$-like state. Keeping that observation in mind, we note that our calculations predict that the $^1A_g^{*-}$-like state is much closer to the $^1B_u^{*+}$-like state in NpSRII (splitting = 0.443 eV, Table 1) and more intense ($f_{calcd} = 0.65$). On

the basis of these results, it is logical to suggest that the $^1A_g^{*-}$-like state might be experimentally observable in the one-photon (normal UV−vis) spectrum. The separation between band C and the absorption maximum of NpSRII is ∼3300 cm^{-1} (0.41 eV), and we suggest that band C represents the absorption maximum of the $^1A_g^{*-}$-like state.

The origin of the vibronic structure in the spectrum of NpSRII is less certain. We speculate that the increased level of vibronic structure is due in part to the loss of Arg-72 dynamic inhomogeneity associated with the position of this residue in a locked electrostatic interaction with Asp-193 (see Figure 3A). In contrast, Arg-82, the corresponding residue in bR, occupies a binding site which has multiple minima with similar energies, but with very different absorption spectra. The mobility of Arg-82, and its spectroscopic consequences, are similar in impact to the mobility of the β-ionylidene ring of the chromophore in rhodopsin (*63*). However, since R82A in BR does not exhibit fine structure (*64*), the above explanation is not sufficient to explain the vibronic structure entirely. We believe that a significant source of the decreased inhomogeneity in NpSRII is associated with a more rigid counterion and water environment near the Schiff base. From another perspective, the quadrapole counterion environment of bR will enhance inhomogeneity due to the flexibility such a structure provides for the central (in this case negative) components (Asp-85 and Asp-212).

ACKNOWLEDGMENT

REFERENCES

1. Spudich, J. L., Yang, C. S., Jung, K. H., and Spudich, E. N. (2000) *Annu. Rev. Cell Dev. Biol. 16*, 365−392.
2. Béjà, O., Aravind, L., Koonin, E., Suzuki, M., Hadd, A., Nguyen, L., Joanovich, S., Gates, C., Feldman, R., Spudich, J., Spudich, E., and DeLong, E. (2000) *Science 289*, 1902−1906.
3. Hoff, W. D., Jung, K. H., and Spudich, J. L. (1997) *Annu. Rev. Biophys. Biomol. Struct. 26*, 223−258.
4. Oesterhelt, D. (1998) *Curr. Opin. Struct. Biol. 8*, 489−500.
5. Lanyi, J. K. (2000) *J. Phys. Chem. B 104*, 11441−11448.
6. Birge, R. R., and Vought, B. W. (2000) in *Methods in Enzymology* (Palczewski, K., Ed.) pp 143−163, Academic Press, San Diego.
7. Ebrey, T., and Koutalos, Y. (2001) *Prog. Retinal Eye Res. 20*, 49−94.
8. Takahashi, T., Yan, B., Mazur, P., Derguini, F., Nakanishi, K., and Spudich, J. L. (1990) *Biochemistry 29*, 8467−8474.
9. Takahashi, T. (1991) *NATO ASI Ser. A211*, 249−256.
10. Imamoto, Y., Schichida, Y., Hirayama, J., Tomioka, H., Kamo, N., and Yoshizawa, T. (1992) *Photochem. Photobiol. 56*, 1129−1134.
11. Tomioka, H., and Sasabe, H. (1995) *Biochim. Biophys. Acta 1234*, 261−267.
12. Chizhov, I., Schmies, G., Seidel, R., Sydor, J. R., Luttenberg, B., and Engelhard, M. (1998) *Biophys. J. 75*, 999−1009.
13. Birge, R. R. (1981) *Annu. Rev. Biophys. Bioeng. 10*, 315−354.
14. Birge, R. R. (1990) *Biochim. Biophys. Acta 1016*, 293−327.
15. Stuart, J. A., and Birge, R. R. (1996) in *Biomembranes* (Lee, A. G., Ed.) pp 33−140, JAI Press, London.
16. Shimono, K., Iwamoto, M., Sumi, M., and Kamo, N. (2000) *Photochem. Photobiol. 72*, 141−145.

17. Luecke, H., Schobert, B., Lanyi, J. K., Spudich, E. N., and Spudich, J. L. (2001) *Science 293*, 1499−1503.
18. Hayashi, S., Tajkhorshid, E., Pebay-Peyroula, E., Royant, A., Landau, E. M., Navarro, J., and Schulten, K. (2001) *J. Phys. Chem. B* (in press).
19. Gellini, C., Luttenberg, B., Sydor, J., Engelhard, M., and Hildebrandt, P. (2000) *FEBS Lett. 472*, 263−266.
20. Scharf, B., Hess, B., and Engelhard, M. (1992) *Biochemistry 31*, 12486−12492.
21. Scharf, B., Hess, B., and Engelhard, M. (1993) *Biochemistry 32*, 3830.
22. Shimono, K., Iwamoto, M., Sumi, M., and Kamo, N. (1998) *J. Biochem. 124*, 404−409.
23. Shimono, K., Kitami, M., Iwamoto, M., and Kamo, N. (2000) *Biophys. Chem. 87*, 225−230.
24. Baselt, D. R., Fodor, S. P. A., van der Steen, R., Lugtenburg, J., Bogomolni, R. A., and Mathies, R. A. (1989) *Biophys. J. 55*, 193−196.
25. Bergo, V., Spudich, E. N., Scott, K. L., Spudich, J. L., and Rothschild, K. J. (2000) *Biochemistry 39*, 2823−2830.
26. Hirayama, J., Imamoto, Y., Shichida, Y., Kamo, N., Tomioka, H., and Yoshizawa, T. (1992) *Biochemistry 31*, 2093−2098.
27. Hirayama, J., Imamoto, Y., Shichida, Y., Yoshizawa, T., Asato, A. E., Liu, R. S., and Kamo, N. (1994) *Photochem. Photobiol. 60*, 388−393.
28. Hirayma, J., Kamo, N., Imamoto, Y., Shichida, Y., and Yoshizawa, T. (1995) *FEBS Lett. 364*, 168−170.
29. Losi, A., Wegener, A. A., Engelhard, M., Gartner, W., and Braslavsky, S. E. (1999) *Biophys. J. 77*, 3277−3286.
30. Losi, A., Wegener, A. A., Engelhard, M., Gartner, W., and Braslavsky, S. E. (2000) *Biophys. J. 78*, 2581−2589.
31. Rath, P., Spudich, E., Neal, D., Spudich, L., and Rothschild, K. (1996) *Biochemistry 35*, 6690−6696.
32. Spudich, J. L., McCain, D. A., Nakanishi, K., Okabe, M., Shimizu, N., Rodman, H., Honig, B., and Bogomolni, R. A. (1986) *Biophys. J. 49*, 479−483.
33. Wada, A., Akai, A., Goshima, T., Takahashi, T., and Ito, M. (1998) *Bioorg. Med. Chem. Lett. 8*, 1365−1368.
34. Zhu, J., Spudich, E. N., Alam, M., and Spudich, J. L. (1997) *Photochem. Photobiol. 66*, 788−791.
35. Yan, B., Spudich, J. L., Mazur, P., Vunnam, S., Derguini, F., and Nakanishi, K. (1995) *J. Biol. Chem. 270*, 29668−29670.
36. Royant, A., Nollert, P., Edman, K., Neutze, R., Landau, E. M., Pebay-Peyroula, E., and Navarro, J. (2001) *Proc. Natl. Acad. Sci. U.S.A.* (in press).
37. Brooks, B., Bruccoleri, R. E., Olafson, B. D., States, D. J., Swaminathan, S., and Karplus, M. (1983) *J. Comput. Chem. 4*, 187−217.
38. Stewart, J. J. P. (1996) *Int. J. Quantum Chem. 58*, 133−146.
39. Stewart, J. J. P. (1997) *THEOCHEM*, 195−205.
40. Stewart, J. J. P. (1999) *MOPAC*, Fujitsu Limited, Tokyo.
41. Hehre, W. J., Yu, J., Klunzinger, P. E., and Lou, L. (1998) *A Brief Guide to Molecular Mechanics and Quantum Chemical Calculations*, Wavefunction, Inc., Irvine, CA.
42. Kusnetzow, A., Singh, D. L., Martin, C. H., Barani, I., and Birge, R. R. (1999) *Biophys. J. 76*, 2370−2389.
43. Kusnetzow, A., Dukkipati, A., Babu, K. R., Singh, D., Vought, B. W., Knox, B. E., and Birge, R. R. (2001) *Biochemistry 40*, 7832−7844.
44. Luecke, H., Schobert, B., Richter, H. T., Cartailler, J. P., and Lanyi, J. K. (1999) *J. Mol. Biol. 291*, 899−911.
45. Martin, C. H., and Birge, R. R. (1998) *J. Phys. Chem. A 102*, 852−860.
46. Tallent, J. R., Stuart, J. A., Song, Q. W., Schmidt, E. J., Martin, C. H., and Birge, R. R. (1998) *Biophys. J. 75*, 1619−1634.
47. Hudson, B. S., and Birge, R. R. (1999) *J. Phys. Chem. 103*, 2274−2281.
48. Vought, B. W., Dukkipatti, A., Max, M., Knox, B. E., and Birge, R. R. (1999) *Biochemistry 38*, 11287−11297.
49. Palczewski, K., Kumasaka, T., Hori, T., Behnke, C. A., Motoshima, H., Fox, B. A., Le Trong, I., Teller, D. C., Okada, T., Stenkamp, R. E., Yamamoto, M., and Miyano, M. (2000) *Science 289*, 739−745.
50. Kochendoerfer, G. G., Wang, Z., Oprian, D. D., and Mathies, R. A. (1997) *Biochemistry 36*, 6577−6587.
51. Tallent, J. R., Birge, J. R., Zhang, C. F., Wenderholm, E., and Birge, R. R. (1992) *Photochem. Photobiol. 56*, 935−952.
52. Liptay, W. (1966) in *Modern Quantum Chemistry* (Sinanoglu, O., Ed.) pp 173−197, Academic Press, New York.
53. Kliger, D. S., Milder, S. J., and Dratz, E. A. (1977) *Photochem. Photobiol. 25*, 277−286.
54. Houjou, H., Inoue, Y., and Sakurai, M. (2001) *J. Phys. Chem. B 105*, 867−879.
55. Murrell, J. N. (1963) *The Theory of the Electronic Spectra of Organic Molecules*, Chapman and Hall Ltd., London.
56. Beppu, Y., and Kakitani, T. (1994) *Photochem. Photobiol. 59*, 660−669.
57. McMeekin, T. L., Groves, M. L., and Hipp, N. J. (1964) in *Amino Acids and Serum Proteins* (Stekol, J. A., Ed.) pp 54−66, American Chemical Society, Washington, DC.
58. Jones, D. D. (1975) *J. Theor. Biol. 50*, 167−183.
59. Chothia, C. (1984) *Annu. Rev. Biochem. 53*, 537−572.
60. Zhang, C., Song, Q. W., Ku, C. Y., Gross, R. B., and Birge, R. R. (1994) *Opt. Lett. 19*, 1406−1411.
61. Myers, A., and Birge, R. (1981) *J. Am. Chem. Soc. 103*, 1881−1885.
62. Birge, R. R., and Zhang, C. F. (1990) *J. Chem. Phys. 92*, 7178−7195.
63. Birge, R. R., Bocian, D. F., and Hubbard, L. M. (1982) *J. Am. Chem. Soc. 104*, 1196.
64. Govindjee, R., Misra, S., Balashov, S. P., Ebrey, T. G., Crouch, R. K., and Menick, D. R. (1996) *Biophys. J. 71*, 1011−1023.